Microlens-aided focusing of linearly and azimuthally polarized laser light

S.S. STAFEEV,[1,2,*] A.G. NALIMOV,[1,2] M.V. KOTLYAR,[2] D. GIBSON,[3] S. SONG,[3] L. O'FAOLAIN,[4,5,6] AND V.V. KOTLYAR[1,2]

[1]*Image Processing Systems Institute—Branch of the Federal Scientific Research Centre "Crystallography and Photonics" of the Russian Academy of Sciences, 151 Molodogvardeyskaya St., Samara 443001, Russia*
[2]*Samara National Research University, 34 Moskovskoye Shosse, Samara 443086, Russia*
[3] *SUPA, Institute of Thin Films, Sensors & Imaging, University of the West of Scotland, High Street, Paisley, PA1 2BE, United Kingdom*
[4]*SUPA, School of Physics and Astronomy of the University of St. Andrews, North Haugh, St. Andrews, KY16 9SS Scotland, UK*
[5]*Tyndall National Institute, Lee Maltings Complex, Dyke Parade, Cork, Ireland*
[6]*Centre for Advanced Photonics and Process Analysis, Cork Institute of Technology, Cork, Ireland*
*[*sergey.stafeev@gmail.com](mailto:sergey.stafeev@gmail.com)*

Abstract: We have investigated a four-Sector transmission Polarization Converter (4-SPC) for a wavelength of 633 nm, that enables the conversion of a linearly polarized incident beam into a mixture of linearly and azimuthally polarized beams. It was numerically shown that by placing a Fresnel zone plate of focal length 532 nm immediately after the 4-SPC, the incident light can be focused into an oblong subwavelength focal spot whose size is smaller than the diffraction limit (with width and breadth, respectively, measuring FWHM = 0.28λ and FWHM = 0.45λ, where λ is the incident wavelength and FWHM stands for full-width at half maximum of the intensity). After passing through the 4-SPC, light propagates in free space over a distance of 300 μm before being focused by a Fresnel zone plate (ZP), resulting in focal spot measuring 0.42λ and 0.81λ. The focal spot was measured by a near-field microscope SNOM, and the transverse E-field component of the focal spot was calculated to be 0.42λ and 0.59λ. This numerical result was verified experimentally, giving a focal spot of smaller and larger size, respectively, measuring 0.46λ and 0.57λ. To our knowledge, this is the first implementation of polarization conversion and subwavelength focusing of light using a pair of transmission micro-optic elements.

OCIS codes: (050.1380) Binary optics; (050.1965) Diffractive lenses; (050.6624) Subwavelength structures; (180.4243) Near-field microscopy; (220.4000) Microstructure fabrication; (230.5440) Polarization-selective devices; (260.5430) Polarization.

References and links

1. N. Yu and F. Capasso, "Flat optics with designer metasurfaces," Nat. Mater. **13**, 139-150 (2014).
2. A.V. Kildishev, A. Boltasseva, and V.M. Shalaev, "Planar photonics with metasurfaces," Science **339**, 1232009 (2013).
3. V.V. Kotlyar and O.K. Zalyalov, "Design of diffractive optical elements modulating polarization," Optik **103**, 125-130 (1996).
4. Z. Bomzon, V. Kleiner, and E. Hasman, "Pancharatnam–Berry phase in space-variant polarization-state manipulations with subwavelength gratings," Opt. Lett. **26**, 1424-1426 (2001).
5. Z. Bomzon, G. Biener, V. Kleiner, and E. Hasman, "Radially and azimuthally polarized beams generated by space-variant dielectric subwavelength gratings," Opt. Lett. **27**, 285-287 (2002).
6. G.M. Lerman and U. Levy, "Generation of a radially polarized light beam using space-variant subwavelength gratings at 1064 nm," Opt. Lett. **33**, 2782-2784 (2008).
7. G.M. Lerman and U. Levy, "Radial polarization interferometer," Opt. Express **17**, 23234-23246 (2009).
8. Z. Ghadyani, I. Vartiainen, I. Harder, W. Iff, A. Berger, N. Lindlein, and M. Kuittinen, "Concentric ring metal grating for generating radially polarized light," Appl. Opt. **50**, 2451-2457 (2011).

9. Z. Xie, J. He, X. Wang, S. Feng, and Y. Zhang, "Generation of terahertz vector beams with a concentric ring metal grating and photo-generated carriers," Opt. Lett. **40**, 359-362 (2015).
10. J. Lin, P. Genevet, M.A. Kats, N. Antoniou, and F. Capasso, “Nanostructured holograms for broadband manipulation of vector beams,” Nano Lett. **13**, 4269-4274 (2013).
11. P. Genevet and F. Capasso, “Holographic optical metasurfaces: a review of current progress,” Rep. Prog. Phys. **78**, 024401 (2015).
12. U. Levy, C.-H. Tsai, L. Pang, and Y. Fainman, "Engineering space-variant inhomogeneous media for polarization control," Opt. Lett. **29**, 1718-1720 (2004).
13. S.S. Stafeev, L. O’Faolain, V.V. Kotlyar, and A.G. Nalimov, "Tight focus of light using micropolarizer and microlens," Appl. Opt. **54**, 4388-4394 (2015).
14. V.V. Kotlyar, S.S. Stafeev, M.V. Kotlyar, A.G. Nalimov, and L. O’ Faolain, "Subwavelength micropolarizer in a gold film for visible light," Appl. Opt. **55**, 5025-5032 (2016).
15. S.S. Stafeev, M.V. Kotlyar, L. O’Faolain, A.G. Nalimov, and V.V. Kotlyar, "Four-sector transmission azimuthal micropolarizer with a phase shift," Comput. Opt. **40**, 12-18 (2016).
16. ET.F. Rogers, S. Savo, J. Lindberg, T. Roy, M.R. Dennis, and N.I. Zheludev, "Super-oscillatory optical needle," Appl. Phys. Lett. **102**, 031108 (2013).
17. F. Qin, K. Huang, J. Wu, J. Jiao, X. Luo, C. Qiu, and M. Hong, "Shaping a subwavelength needle with ultra-long focal length by focusing azimuthally polarized light," Sci. Rep. **5**, 09977 (2015).
18. G. Yuan, E.T.F. Rogers, T. Roy, G. Adamo, Z. Shen, and N.I. Zheludev, "Planar super-oscillatory lens for sub-diffraction optical needle at violet wavelengths," Sci. Rep. **4**, 6333 (2014).
19. E.T.F. Rogers, J. Lindberg, T. Roy, S. Savo, J.E. Chad, M.R. Dennis, and N.I. Zheludev, "A super-oscillatory lens optical microscope for subwavelength imaging," Nat. Mater. **11**, 432-435 (2012).
20. G. Chen, K. Zhang, A. Yu, X. Wang, Z. Zhang, Y. Li, Z. Wen, C. Li, L. Dai, S. Jiang, and F. Lin, "Far-field sub-diffraction focusing lens based on binary amplitude-phase mask for linearly polarized light," Opt. Express **24**, 11002-11008 (2016).
21. D. Tang, C. Wang, Z. Zhao, Y. Wang, M. Pu, X. Li, P. Gao, and X. Luo, "Ultrabroadband superoscillatory lens composed by plasmonic metasurfaces for subdiffraction light focusing," Las. Photon. Rev. **9**, 713-719 (2015).
22. G. Chen, Y. Li, A. Yu, Z. Wen, L. Dai, L. Chen, Z. Zhang, S. Jiang, K. Zhang, X. Wang, and F. Lin, "Super-oscillatory focusing of circularly polarized light by ultra-long focal length planar lens based on binary amplitude-phase modulation," Sci. Rep. **6**, 29068 (2016).
23. N. Davidson and N. Bokor, "High-numerical-aperture focusing of radially polarized doughnut beams with a parabolic mirror and a flat diffractive lens," Opt. Lett. **29**, 1318-1320 (2004).
24. X. Li, Y. Cao, N. Tian, L. Fu, and M. Gu, "Multifocal optical nanoscopy for big data recording at 30 TB capacity and gigabits/second data rate," Optica **2**, 567-570 (2015).
25. X. Hao, C. Kuang, T. Wang, and X. Liu, "Phase encoding for sharper focus of the azimuthally polarized beam," Opt. Lett. **35**, 3928-3930 (2010).
26. S. Wang, X. Li, J. Zhou, and M. Gu, "Ultralong pure longitudinal magnetization needle induced by annular vortex binary optics," Opt. Lett. **39**, 5022-5025 (2014).
27. C. M. Sundaram, K. Prabakaran, P. M. Anbarasan, K. B. Rajesh, and A. M. Musthafa “Creation of Super Long Transversely Polarized Optical Needle Using Azimuthally Polarized Multi Gaussian Beam,” Chinese Phys. Lett. **33**(6), 064203 (2016).
28. K. Debnath, L. O'Faolain, F. Y. Gardes, A. G. Steffan, G. T. Reed, and T. F. Krauss "Cascaded modulator architecture for WDM applications," Opt. Express **20**, 27420-27428 (2012).
29. V.V. Kotlyar, S.S. Stafeev, Y. Liu, L. O’Faolain, and A.A. Kovalev, "Analysis of the shape of a subwavelength focal spot for the linearly polarized light," Appl. Opt. **52**, 330-339 (2013).

---

1. Introduction

Recent years have seen an increased interest of the research community in the study of metasurfaces – elements enabling the manipulation of the amplitude, phase and polarization of optical beams (see review articles [1, 2]). In the particular case of the metasurface, diffraction gratings with subwavelength features have been realized [3] which are suitable for polarization control of a passing light beam.

The first subwavelength binary micropolarizers to be manufactured operated in the IR range [4, 5], implementing conversion of circularly polarized light of wavelength 10.6 µm into an azimuthally polarized beam. Generation of a radially polarized laser beam using a subwavelength diffraction grating operating at 1064 nm has also been reported [6]. A radial polarization interferometer that employs the subwavelength grating described in [6] has also been reported [7].

A concentric-ring metal grating for generating radially polarized light of wavelength 633 nm from a circularly polarized beam has been discussed [8]. Using a similar approach, a terahertz vector radially polarized beam was generated in [9]. However, it is worthwhile noting that the beam discussed in [8] cannot be defined as being radially polarized in a strict sense. While being characterized by the radial polarization vector and a doughnut transverse intensity pattern, the beam's transverse phase distribution was not uniform. As a remedy for the said drawback, a combined holographic element composed of a concentric metal ring [8] and a "fork" hologram was introduced in [10, 11].

The above-listed articles can be divided in two groups. The first group [4,5,8-11] discusses the conversion of circularly polarized light into cylindrically symmetric beams. Being an analog of quarter-wave plates, such optical elements are easier to fabricate, as the grating microrelief features have a smaller aspect ratio. The second group contains elements intended to transform linearly polarized light into the radially or azimuthally polarized beams [6,7,12]. Such elements can be looked upon as analogs of a half-wave plate.

In earlier publications, we reported on the characterization of four-sector subwavelength gratings for incident light polarization manipulation. The reflective four-Sector transmission Polarization Converter (4-SPC) proposed in [13] was intended to convert linearly polarized incident light of wavelength λ into a radially polarized beam, which was then focused into an elongated subwavelength focal spot with smaller and larger sizes, respectively, measuring at full-width half-maximum of intensity FWHM = 0.40λ and FWHM = 0.50λ. In a similar way, reflective [14] and transmission azimuthal micropolarizers [15] have been described. As a follow-up from our previous study [15], in this work we discuss obtaining a tight focal spot by focusing a laser beam transmitted through a 4-SPC.

There are also experimental works on generation of a far-field subwavelength focal spot by using a super-oscillatory lens (SOL) [16-22]. In [16-18] the SOL was used to generate a light needle at a distance of 240λ [17]. The needle had a length of DOF=15λ [16,18] and DOF=12λ [17], as well as a diameter of FWHM=0.42λ [16,17] and FWHM=0.45λ [18] for the visible (λ=633 nm) [16,17] and violet (λ=408 nm) [18] light. However, the side lobes were up to 50% [17] and focusing efficiency was not high, since the incident beam energy was distributed along the needle. In [19] by using a SOL with a focal distance of *f*=10.3μm a focal spot was obtained with a diameter of FWHM=0.29λ. However, the intensity side lobes exceeded the intensity in focus. In [20] by using a 1D SOL a focal line was generated at a distance of *f*=94 μm with a thickness of FWHM=0.41λ (side lobes were 22%). In [21] an ultrabroadband SOL was studied, which focused the light in the wavelength range from 405 nm to 785 nm. However, the focal spot diameter exceeded the diffraction limit. In [22] a SOL with ultra-long focal length *f*=252.8μm generated a focal spot with a diameter FWHM=0.454λ. However, the efficiency was only about 1% and side lobes were 26%.

Below, we discuss a four-sector transmission micropolarizer that enables the conversion of linearly polarized incident light into an azimuthally polarized beam. The resulting azimuthally polarized beam is characterized by a phase shift of π between the diametrically opposite beam points. Tightly focusing is implemented using a binary Fresnel lens as it enables obtaining a tighter focal spot when compared with an aplanatic lens [23]. Sharply focused azimuthally polarized optical vortices may find prospective uses in optical data storage [24]. We show that by placing a Fresnel zone plate (ZP) of focus 532 nm immediately behind the four-sector micropolarizer, light can be focused into a subwavelength focal spot with smaller and larger sizes measuring FWHM_x = 0.28λ and FWHM_y = 0.45λ, which is below the diffraction limit. It is also shown that if after passing through the micropolarizer the beam is allowed to propagate in free space over a distance of 300 μm before being focused by the ZP, the focal spot has respective sizes FWHM_x = 0.42λ and FWHM_y = 0.81λ (with the contribution of the transverse E-field component being FWHM_x = 0.42λ and FWHM_y = 0.59λ). Note that the experimental verification of the last numerical result has given a focal spot measuring FWHM = 0.46λ and FWHM = 0.57λ. The main advantage of the obtained focus is almost full absence of the side lobes (less than 10%). Note that in the above-mentioned works [16-22] the side lobes level exceeded 20%.

2. Design and fabrication of the 4-SPC

In this work, we fabricated and characterized a visible-range binary subwavelength transmission element with a metasurface that is able to convert linear polarization into inhomogeneous near-azimuthal polarization, with the diametrically opposed beam points being characterized by a phase shift of π. By introducing such a phase shift we have combined a 4-sector azimuthal polarizer and a 4-sector analog of a spiral phase plate in a single element. Previously, an azimuthally polarized laser beam having passed through a spiral phase plate was shown to form a subwavelength focal spot of size below the diffraction limit. In [25] such a beam was shown to produce a focal spot whose area ($0.147\lambda^2$) was 13.5% smaller than a focal spot from a radially polarized beam ($0.17\lambda^2$). In [26] the authors reported focusing an azimuthally polarized beam transmitted through concentric-ring filters, with the rings represented by spiral phase plates arranged so as to provide a phase shift of π between the adjacent rings. Being focused with a wide-NA lens (NA = 0.95) onto a layer of magneto-optical material, such a beam produced a needle-like focus of size FWHM = 0.38λ and depth DOF = 7.48λ. Using a similar structure, a needle-like focus was numerically obtained in [27], measuring FWHM = 0.366λ and DOF = 22λ.

The designed micropolarizer with half-wavelength shift for linear-to-azimuthal polarization conversion contains four sectors, with the subwavelength gratings grooves tilted by -60°, 60°, -60°, and 60°. Depending on which sector the beam is incident on, the polarization direction of linearly polarized light changes by -45°, 45°, -45°, or 45° relative to the incident polarization. The gratings have a 230-nm period, a 138-nm step width, and a 92-nm grove width. The grating was fabricated in an amorphous silicon film. The microrelief height is 130 nm, the operating wavelength is 633 nm, and the complex refractive index of silicon is given by $n = 3.87 - 0.016i$ (measured using ellipsometry). It was found that just 15% of the incident beam energy passed through the micropolarizer. The relatively low efficiency is due to absorption of light in silicon. At the same time, the high-contrast refractive index of silicon enabled the microrelief height to be reduced by a factor of 2.6, which is significant considering the groove width under 100-nm. The fabricated micropolarizer measures 100×100 µm. In our earlier papers [13-15] we showed that it would suffice to use a 4-sector polarizer to generate a cylindrical vector beam.

The fabricated micropolarizer in Fig. 1 has parameters slightly different from the calculated ones, having a 244-nm period, a 148-nm step width, and a 96-nm groove width. Note, however, that such a discrepancy falls within 6%. The micropolarizer in Fig. 1 was fabricated by electron beam lithography. The surface of a 130-nm thick amorphous silicon (a-Si) found on a transparent pyrex 7740 substrate (refractive index is 1.47, http://www.valleydesign.com/pyrex.htm) was coated with a 320-nm thick PMMA resist, which was then baked at 180 °C. To prevent charging the sample surface was coated with a 15-nm thick golden layer. The 4-sector grating-polarizer's pattern was created on the resist surface by a 30-kV electron beam. The sample was developed in a 3:7 water solution of isopropanol and the gold layer removed. The transfer of the grating-polarizer's template from the resist to the aSi was carried out via reactive ion etching in the gas mixture of CHF_3 and SF_6 using a recipe optimized for photonic crystal fabrication similar to that used in [28] The resist thickness was chosen so as to enable the protection of pattern during the etching of the 130-nm aSi. The aspect ratio of etch rates of the material and the mask was found to be 1:2.5.

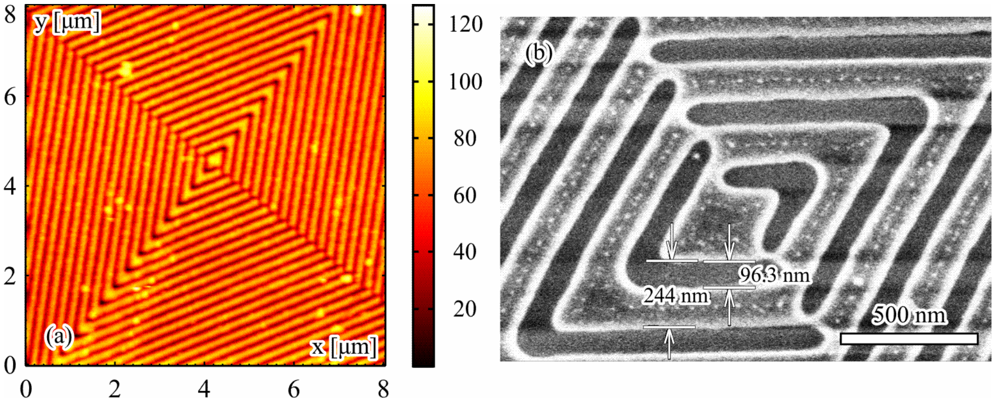

Fig. 1. Atomic-force-microscope (a) and scanning electron microscope (b) images of the central part of the transmission 4-SPC. The scale shows the microrelief depth in nm.

3. Modeling the propagation of light through the 4-SPC

The performance of a perfect micropolarizer (with no regard for fabrication errors) was modeled as follows: the field transmitted through the element was calculated using the FDTD method implemented in the FullWAVE software (https://optics.synopsys.com/rsoft/rsoft-passive-device-fullwave.html). The element's microrelief was assumed to be illuminated via the substrate by a linearly polarized plane wave of wavelength $\lambda = 633$ nm at normal incidence. In the FDTD modeling, the grid step was equal to $\lambda/30$. The relief height was taken to be 130 nm. The refractive index of the substrate was $n = 1.5$. The far field intensity distribution was calculated using vector Rayleigh-Sommerfeld integrals, with the FDTD-aided field intensity 100-nm away from the micropolarizer's surface used as the initial distribution. Figure 2 shows the intensity pattern and polarization vectors of the light transmitted through the micropolarizer. By way of illustration, Figs. 3, 4 depict the intensity patterns that would result from passing the light filed in Fig. 2 via polarizer-analyzers rotated by 0°, 45°, -45°, and 90° relative to the polarization direction of the incident beam. The intensity patterns in Figs. 3,4 were calculated using Jones matrices.

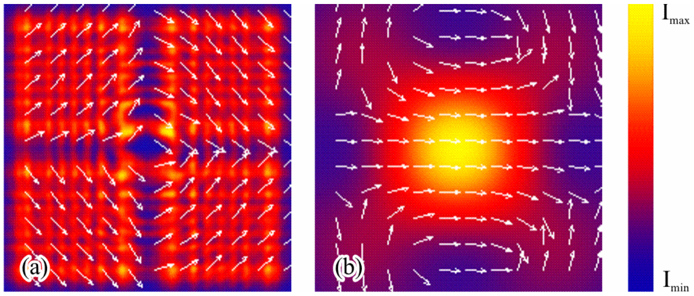

Fig. 2. Intensity pattern (negative) and polarization vectors for a beam transmitted through the micropolarizer, generated 5.1-μm (a) and 300- μm (b) away from its surface. The image size is 10×10 μm.

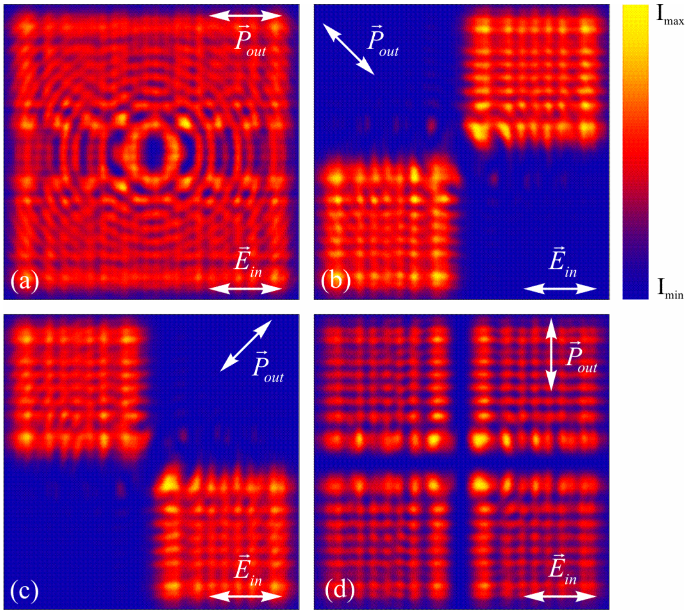

Fig. 3. Intensity distribution (negative) for a beam $\vec{E}_{in}$ having passed through a micropolarizer, measured 5.1-µm away from the micropolarizer surface. The analyzer $\vec{P}_{out}$ is rotated by 0° (a), -45° (b), 45° (c), and 90° (d) with respect to the polarization vector $\vec{E}_{in}$.

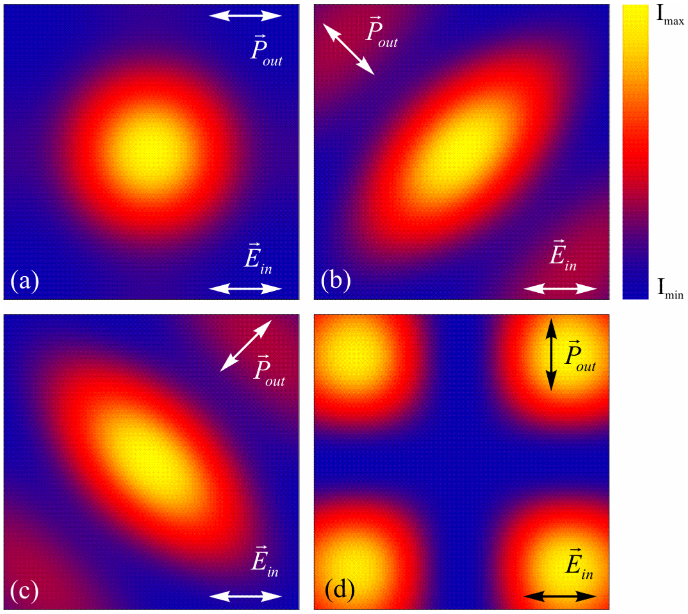

Fig. 4. Intensity distribution (negative) for a beam $\vec{E}_{in}$ having passed through a micropolarizer, measured 300-µm away from the micropolarizer surface. The analyzer $\vec{P}_{out}$ is rotated by 0° (a), -45° (b), 45° (c), and 90° (d) with respect to the polarization vector $\vec{E}_{in}$.

From Fig. 2, in the near field (5.1-μm away from the micropolarizer) the polarization is seen to be near-azimuthal. Closer to the far field (at a 300-μm distance, Fig. 4), the field amplitude has a central maximum. Thus the modeling has shown that a micropolarizer with phase shift from Fig. 1 is able to generate in the near field a beam with near azimuthal polarization, characterized by a phase shift of π in the diametrically opposite points. This leads to the central maximum in the far field.

4. Simulation of focusing of light after passing 4-SPC by a Fresnel ZP

At the first stage of our study, we numerically simulated the focusing of laser light of wavelength λ = 633 nm, having passed through a four-sector micropolarizer, by means of a Fresnel ZP of focus f = 532 nm. The reason for using the Fresnel ZP as a focusing element was that given identical numerical apertures (NA) it enables the realization of a tighter focal spot when compared with an aplanatic lens [23]. The incident wavelength was chosen more than the focal length of the ZP to reduce the focal length.

The parameters of the ZP from Fig. 5 used in simulation were the same as those of the real Fresnel ZP that was later utilized in the experiment. The ZP of diameter 14 μm had a microrelief depth of 510 nm. Being composed of 12 rings and a central disk, the ZP was assumed to be fabricated in a resist with refractive index 1.52. The simulated ZP was entirely made of the resist, i.e. the substrate had a refractive index equal to that of the ZP.

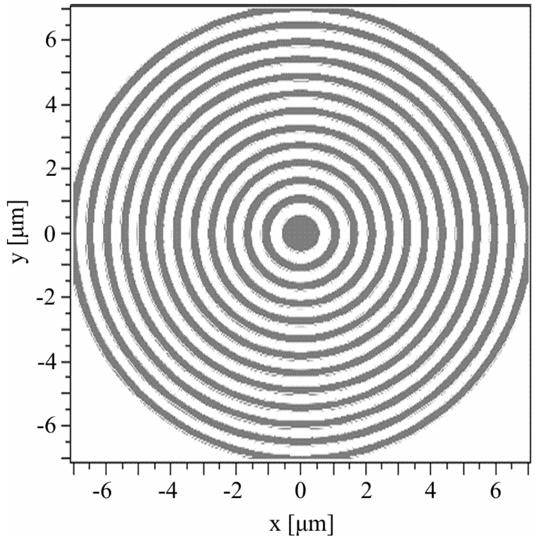

Fig. 5. The Fresnel ZP under simulation as seen in a FullWave window.

The beam incident on the ZP from Fig. 5 was assumed to have a complex amplitude distribution shown in Figs. 2(b) and 4. Figures 6-8 depict the simulation results. Figure 6 depicts the calculated intensity patterns in the (a) parallel and (b) perpendicular planes relative to the polarization direction of the incident beam. Figure 7 shows the intensity profile along the optical axis. The intensity profiles along the y- and x-axes in the focal plane are shown in Fig. 8. An elliptic focal spot is seen to have smaller and larger sizes measuring $\mathrm{FWHM}_x = 0.42\lambda$ and $\mathrm{FWHM}_y = 0.81\lambda$. The transverse dimensions of the focal spot along the Cartesian coordinates (x,y) at a distance of z=250 nm from the ZP were calculated at half-maximum of intensity. The focus was generated at a smaller distance than the focal distance of the ZP (f=532 nm). Note that while taking into account only the transverse E-field component, the larger size of the spot is 0.59λ (dashed line in Fig. 8(a)), since the tip used in this work near-field optical microscope NSOM is sensitive only to the transverse intensity. The area below the horizontal dashed line in Fig. 8 consists of material the refractive index of

1.52. Taking the substrate into account leads to increasing of the focal spot size. Simulation without the ZP substrate is described below in Section 6.

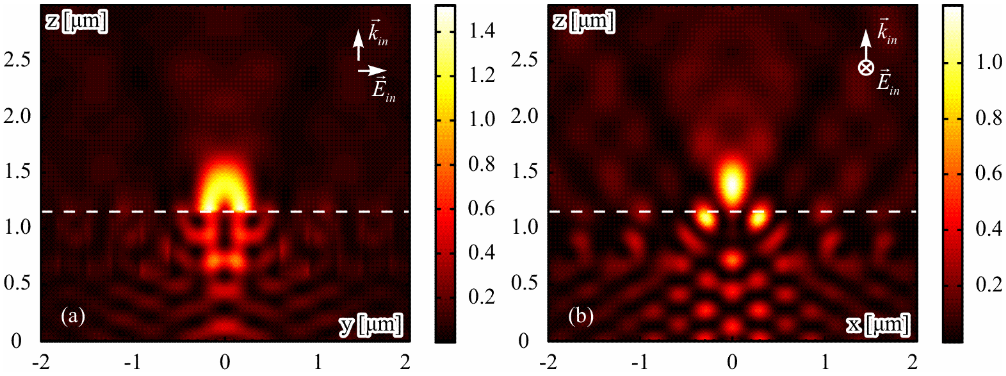

Fig. 6. Intensity patterns within the calculation domain in the (a) YZ- and (b) XZ-planes. ZP boundary is marked with the dashed line.

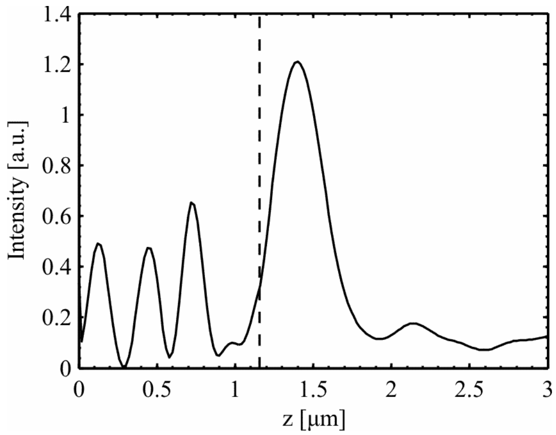

Fig. 7. Intensity profile along the z-axis. ZP boundary is marked with the black dashed line.

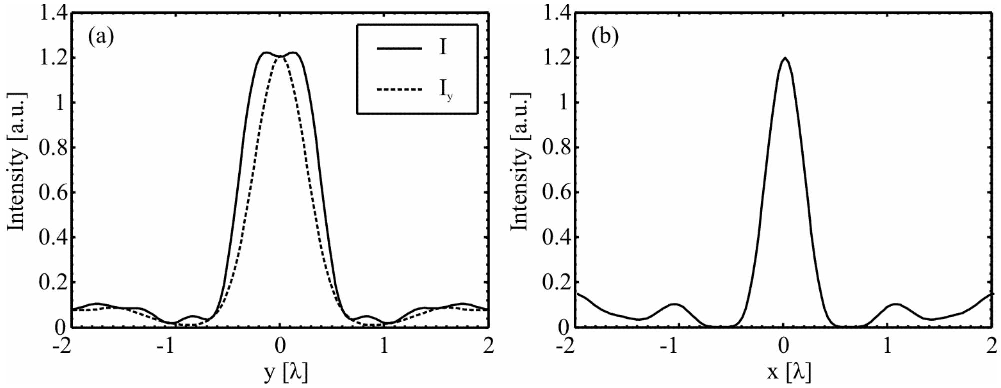

Fig. 8. Intensity profiles in the focal spot along the (a) y- and (b) x-axes. The total intensity is marked with the solid line and the transverse intensity component is marked with the dashed line.

5. Experiment

In the experiment, a laser beam of wavelength λ = 633 nm was focused with a ZP of focal length *f* = 532 nm after having passed through a 4-SPC.

The optical arrangement for the experimental measurements is shown in Fig. 9(a). Linearly polarized laser light from a 55 mW He-Ne laser of wavelength 633 nm was delivered via an optical fiber to a substrate containing a 4-SPC on its surface. The 4-SPC under study was rigidly attached to the other substrate (thickness is 0.5mm) containing an array of ZPs from Fig. 9(b) [13]. For ease of understanding, the ZP and 4-SPC are separated by a distance in Fig. 9(a).

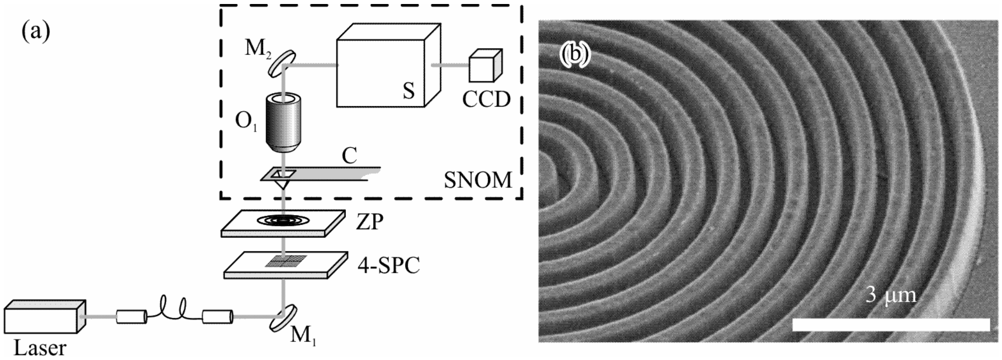

Fig. 9. Experimental optical arrangement (a): M_1, M_2 are mirrors, O_1 is a 100× objective, C is a probe, S is a spectrometer, and CCD is a video-camera. SEM image of ZP [13] (b).

Note that while the substrate contained many zone plates, each with different fillfactor, only a single zone plate was used in each run of the experiments. The ZP and 4-SPC were superimposed using a conventional optical microscope. Shown in Fig. 10(b) is an optical microscope image of the ZP against the background of a 4-SPC. Note that superposition of the 4-SPC and ZP centers is a critical operation, and the focusing result depends on the accuracy of this alignment. A number of arrangements were chosen and the best focusing result shown below. The alignment tolerances are within those provide by pick and place assembly tools which could be used for mass manufacture. The inset in Fig. 10 shows a magnified image in an optical microscope of the exactly aligned 4-SPC and ZP.

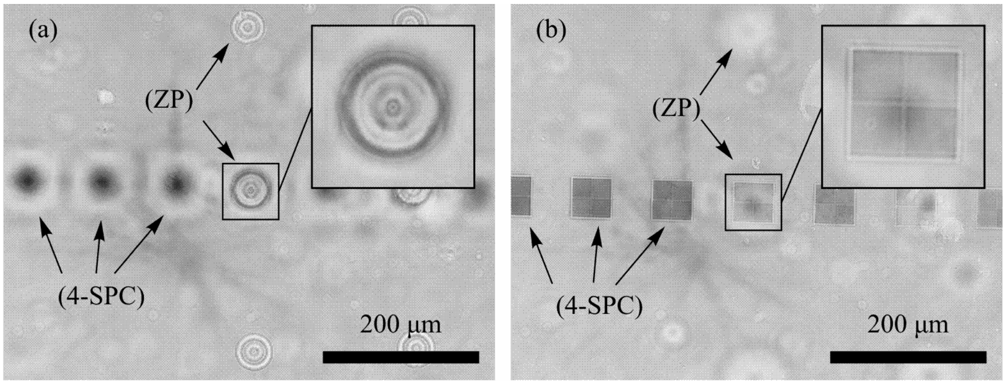

Fig. 10. An optical microscope 20x image of (a) a ZP on the 4-SPC background and (b) a 4-SPC on the ZP background. The inset shows magnified and aligned ZP and 4-SPC with their centers lying on the optical axis.

The location of the focal spot on the ZP and its size were controlled by shifting the mirror M_1. After passing through the 4-SPC, the beam was focused with the ZP. The intensity distribution in the focal spot was measured at different distances from the ZP surface with a hollow metal pyramid taper *C*. There was a 100-nm pinhole in the taper tip. Having passed through the taper's pinhole, the light then traveled to a 100× objective

O_1, before being transmitted through a spectrometer (Solar TII, Nanofinder 30) to filter off unwanted noise and registered by a CCD-camera (Andor, DV401-BV).

To ascertain that the beam has passed through the 4-SPC, a conventional polarizer can be placed after the objective O_1. Figure 11 shows images of the transmitted beam for different positions of the polarizer. The images are identical to those reported earlier in [15]. From the similarity of the images in Figs. 4 and 11, we can be sure that prior to hitting the ZP, radiation passes through the 4-SPC. For ease of comparison, the insets in Fig. 11 show the calculated intensity distributions, taken from Fig. 4. It is seen that the experimental beam patterns are consistent with the simulation.

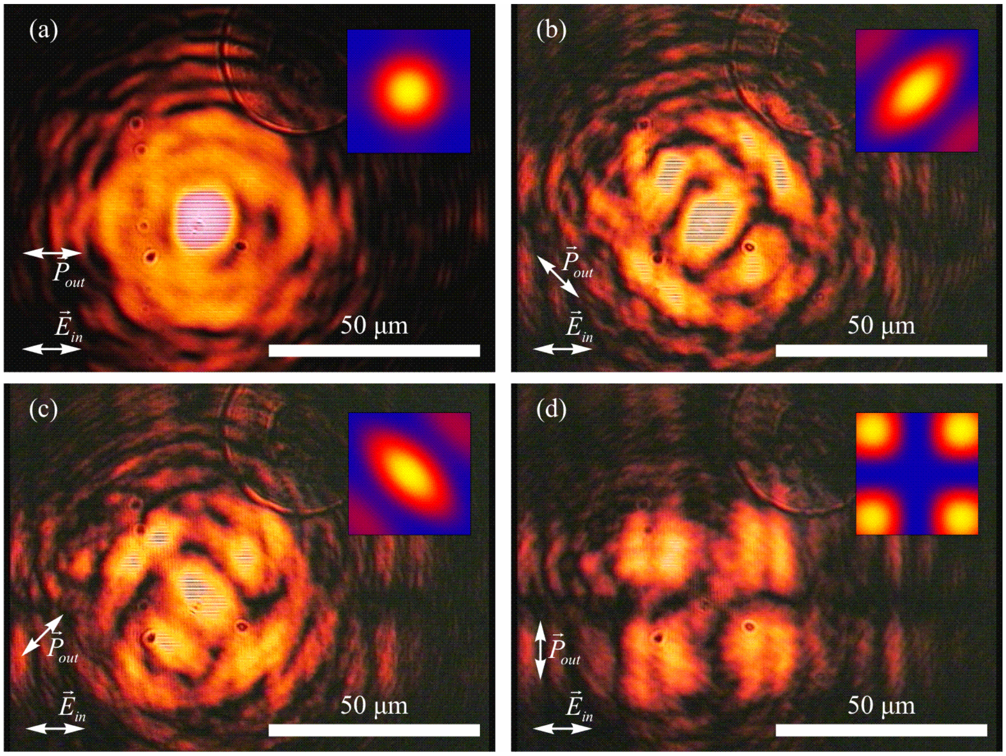

Fig. 11. Images of the transmitted beam $\vec{E}_{in}$ obtained at different polarizer positions $\vec{P}_{out}$: 0 (a), -45º (b), 45º (c), and 90º (d). For comparison, the insets show calculated intensity distributions from Fig.4. It is also seen in the figure that the ZP is shifted from the optical axis (the ZP center is marked by the cross).

Measurements with a near-field scanning optical microscope have shown a focal spot to be formed at a distance of 250 nm from the ZP surface, with the spot size having FWHM = 0.46λ and FWHM = 0.57λ. Fig. 12 shows the experimentally measured focal spot and its intensity profiles along the *x*- and *y*-axes. In [29], the Ntegra Spectra microscope that we utilized in the present experiment was shown to predominantly measure the transverse E-field component. The comparison of the experimentally measured sizes of the focal spot (FWHM = 0.46λ and FWHM = 0.57λ) and those derived via numerical simulation (FWHM = 0.42λ and FWHM = 0.59λ) for the transverse E-field component (dashed curve in Fig. 8(a)) suggests that they are in agreement.

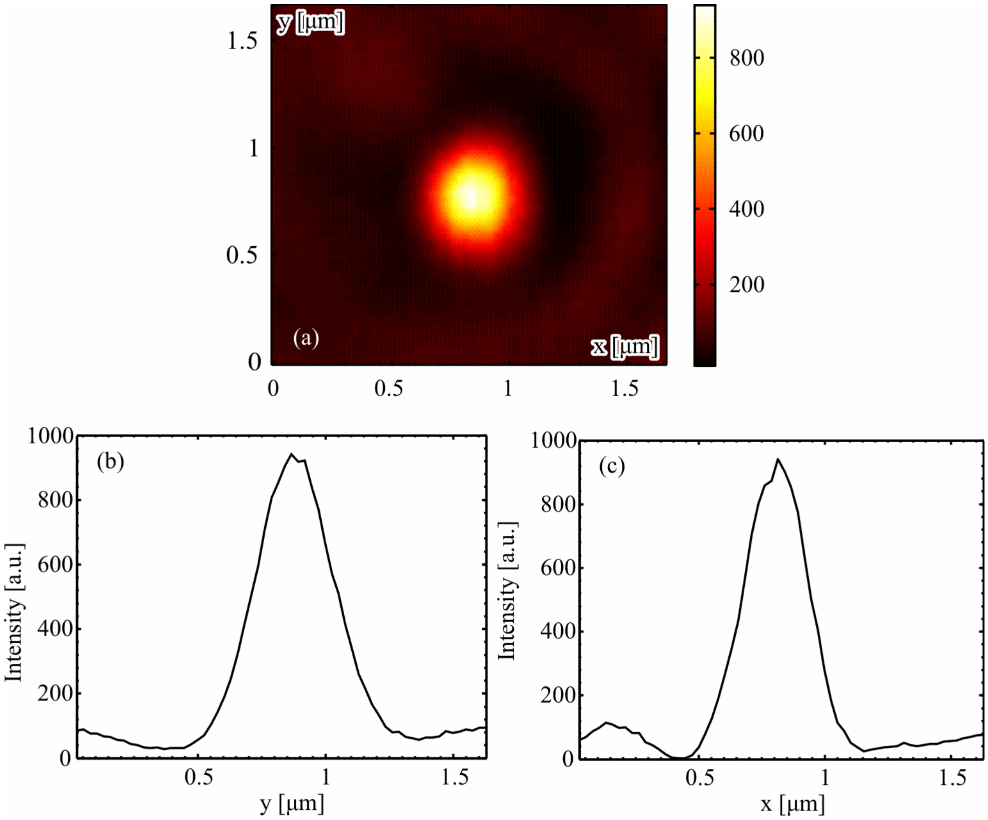

Fig. 12. Intensity profile of the focal spot measured using a NSOM Ntegra Spectra: 2D intensity distribution (a) and intensity profiles along the y- (b) and x-axis (c).

6. Simulation of focusing of light by using the 4-SPC and ZP without the substrate

In this section, the focusing of light of wavelength λ = 633 nm that was passed through a 4-SPC before being focused by a ZP of focus f = 532 nm was numerically simulated. The 4-SPC was assumed to be placed directly in front of the ZP. As was the case in far-field simulation, the ZP parameters were the same as those of a real ZP utilized in the physical experiment. The ZP was assumed to be illuminated by a laser beam whose complex amplitude distribution is shown in Figs . 2(a) and 3.

The simulation results are presented in Figs. 13-15. Figure 13 depicts the intensity patterns in the (a) parallel and (b) perpendicular planes with respect to the incident beam polarization. Figure 14 shows the intensity profile along the optical axis. From Figs. 13-14, an intensity peak (focal spot) is seen to be generated just behind the ZP surface. Figure 15 shows the intensity profiles in the focal plane. The focal spot is elliptic, measuring $\mathrm{FWHM}_x = 0.28\lambda$ and $\mathrm{FWHM}_y = 0.45\lambda$ at a distance of 40 nm from the surface. Note that while taking into account only the transverse E-field component, the size of the larger spot is 0.42λ (dashed line in Fig. 15(a)).

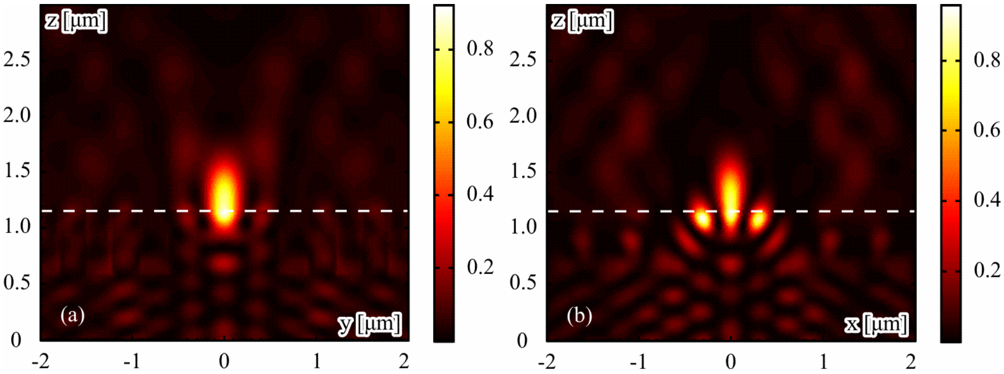

Fig. 13. Intensity pattern in the central part of the calculated domain in the (a) YZ- and (b) XZ-planes. The dotted line marks the ZP surface boundary.

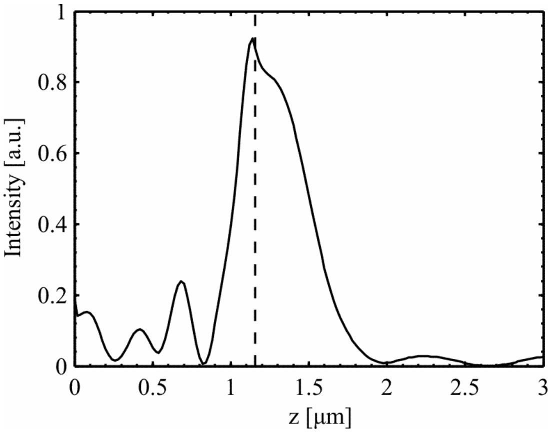

Fig. 14. Intensity profile along the z-axis. Black dashed line marks the ZP relief boundary.

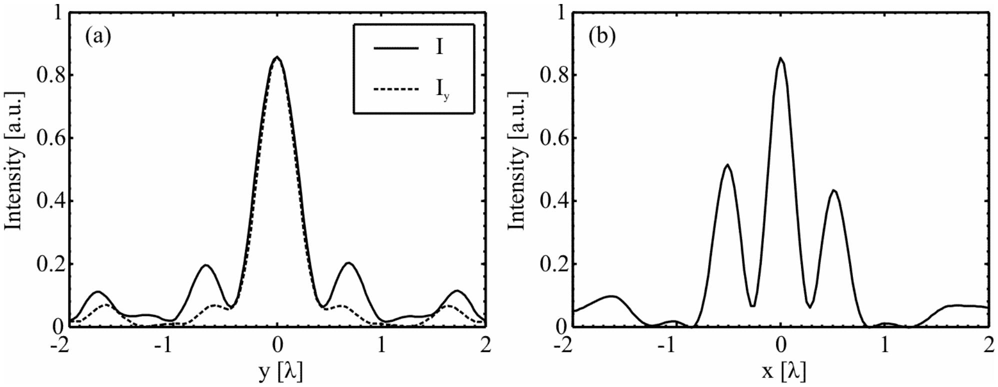

Fig. 15. Intensity profile 40-nm away from the ZP surface along the (a) y- and (b) x-axes. The solid line depicts the total intensity and the dotted line is for the transverse component of the intensity.

With increasing distance from the ZP surface, the focal spot gets larger and more circular, e. g. 200-nm away from its surface the spot size is $\mathrm{FWHM}_x = 0.37\lambda$ and $\mathrm{FWHM}_y = 0.48\lambda$. The intensity profiles 200-nm away from the ZP are depicted in Fig. 16.

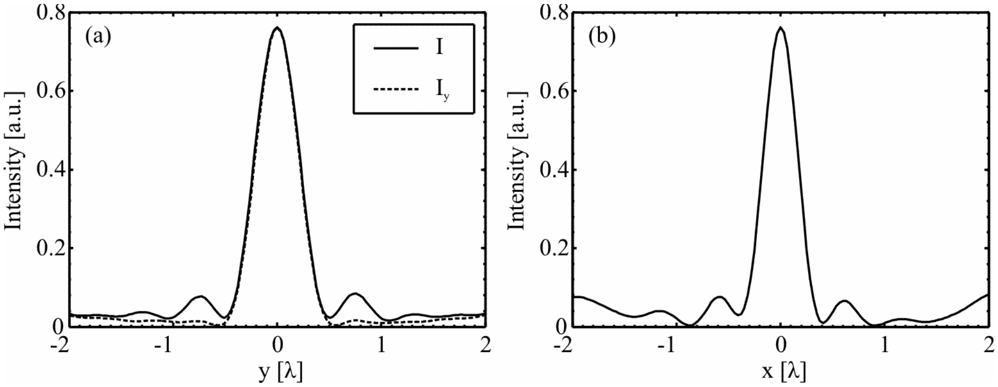

Fig. 16. Intensity profile 200-nm away from the ZP along the (a) y- and (b) x-axes. Solid line depicts the total intensity and the dotted line is for the transverse intensity component.

From Fig. 4, the central part of the beam transmitted through the 4-SPC is seen to be nearly completely linearly polarized along the y-axis, see Fig. 4(e), in the meantime it was an azimuthally polarized beam which was observed at the 4-SPC exit, as shown in Fig. 2(a). As a result, when the 4-SPC -to-ZP distance increases to 300 μm the focal spot increases in size from $\mathrm{FWHM}_x = 0.28\lambda$ and $\mathrm{FWHM}_y = 0.45\lambda$ to $\mathrm{FWHM}_x = 0.42\lambda$ and $\mathrm{FWHM}_y = 0.81\lambda$.

We would like to note that with the ZP being synthesized in a substrate hundreds of micrometers thick, it appeared impossible to place the 4-SPC right up against the ZP. However, this difficulty can be obviated by obtaining a 4-SPC image in front of the ZP relief. In this case, the polarization vector in the image would be the same as that at the 4-SPC exit (see Fig. 11). In this way, it is possible that there exists a coupling between the nanostructures in ZP and 4-SPC. Another approach is to combine the polarizer and the lens in one element. To do this, the grooves of subwavelength gratings of the polarizer from Fig. 1 should be etched within the zones of the microlens from Fig. 5 so as to implement a phase delay of π when passing from one zone of the microlens to another.

7. Conclusion

We have studied a four-sector transmission polarization convertor intended to convert linearly polarized laser light into an azimuthally polarized beam with its phase shifted by π in diametrically opposed points, by applying the proposed micropolarizer for tight focus of light. The results obtained are as follows.

1. FDTD-aided simulation has shown that by illuminating the ZP with a laser beam transmitted through a 4-SPC it is possible to obtain an elliptic subwavelength focal spot whose size is smaller than the diffraction limit, measuring $\mathrm{FWHM}_x = 0.28\lambda$ and $\mathrm{FWHM}_y = 0.45\lambda$.

2. If after passing through the 4-SPC the beam was allowed to propagate in free space over a distance of 300 μm, before being focused by the ZP, the resulting focal spot measured $\mathrm{FWHM}_x = 0.42\lambda$ and $\mathrm{FWHM}_y = 0.81\lambda$. Notably, the spot size contributed to only by the transverse E-field component was $\mathrm{FWHM}_x = 0.42\lambda$ and $\mathrm{FWHM}_y = 0.59\lambda$.

3. The last numerical result above was verified experimentally using NSOM measurements. Experimentally measured size of the focal spot was $\mathrm{FWHM}_x = 0.46\lambda$ and $\mathrm{FWHM}_y = 0.57\lambda$.

Funding

Russian Foundation for Basic Research (RFBR) (14-29-07133, 14-07-97039, 15-07-01174, 15-47-02492, 15-37-20723, 16-07-00990, 16-47-630483); Ministry of Education and Science of the Russian Federation (NSh-4128.2016.9, MK-9019.2016.2); European Research Council (337508).